Proceedings of the 3rd Marine Energy Technology Symposium
METS2015
April 27-29, 2015, Washington, D.C.

# CHARACTERIZATION AND CONTROL OF CROSS-FLOW TURBINE IN SHEAR FLOW

Dominic Forbush[1]
University of Washington
Seattle, WA, United States

Dr. Brian Polagye
University of Washington
Seattle, WA, United States

Dr. Jim Thomson
University of Washington
Seattle, WA, United States

Dr. Brian Fabien
University of Washington
Seattle, WA, United States

James Donegan
Ocean Renewable Power Company
Portland, ME, United States

Jarlath McEntee
Ocean Renewable Power Company
Portland, ME, United States

[1]Corresponding author: forbudom@u.washington.edu

## INTRODUCTION

Hydrokinetic turbines may experience both lateral and vertical sheared inflow. Characterizing and controlling turbines under these conditions is challenging because point measurements cannot provide an adequate reference velocity. This study investigates a helical, fixed pitch, cross-flow turbine (RivGen®) developed by the Ocean Renewable Power Company (ORPC) for operation in riverine environments.

### Turbine Description

The RivGen turbine (Figure 1) measures 11 m in length and has a radius of 0.7 m. It designed for community scale power ~25 kW.

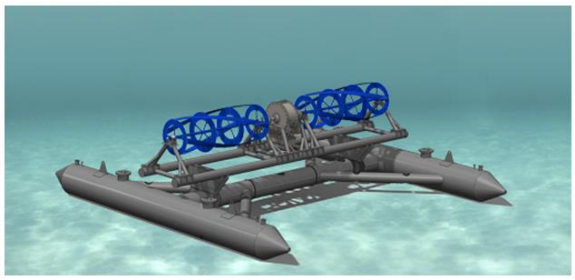

**FIGURE 1. ORPC RIVGEN TURBINE.**

### Site Description

The turbine was deployed in 2014 on the Kvichak River just downstream of the village of Igiugig, AK (USA). At the deployment site, the river is approximately 5 m deep and 150 m wide. The site is described in a coordinate frame oriented with the turbine rotor with $(x,y)=(0,0)$ nominally at the rotor center. $x > 0$ corresponds to the downstream direction and $y > 0$ corresponds to the across-stream direction, towards the village. Doppler velocimeters and current profilers, deployed from upstream vessels, spatially resolved the velocity field in the vicinity of the turbine [1], [2]. At turbine hub height (2.5 m depth), the spatially-resolved profile was found to be synoptic on the order of days to weeks. Lateral shear is significant varying from 1.6 m/s to 2.3 m/s along the rotor span. This represents a 200% increase in kinetic power density. This time-averaged laterally-sheared flow pattern and associated uncertainties are shown as Figure 2. Vertical shear is negligible. A detailed consideration of turbulent inflow conditions in rivers can be found in [3].

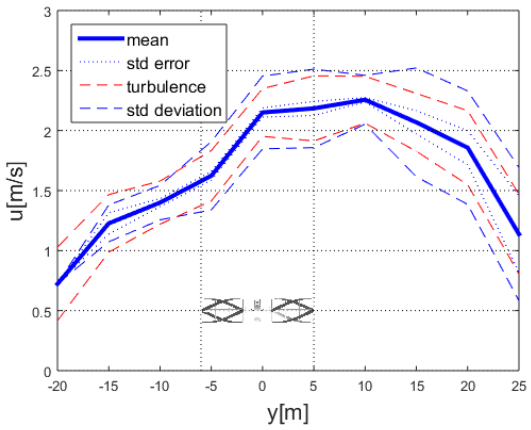


**FIGURE 2. LATERAL SHEAR PROFILE AT TURBINE HUB HEIGHT. TURBINE SUPERIMPOSED TO SCALE.**

Turbulence intensity is consistently 10%. Spectral analysis of Doppler velocimeter data shows that the majority of the energy is contained at $f < 0.2$ Hz [4]. Similar frequency-domain analysis

of the turbine power generation demonstrates that it has similar frequency sensitivity (Figure 3).

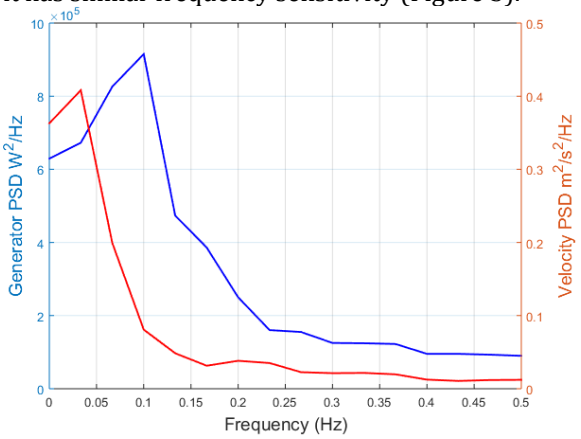


**FIGURE 3. POWER SPECTRA OF INFLOW AND TURBINE POWER OUTPUT.**

## PERFORMANCE CHARACTERACTIZATION

### Methods

The turbine shore station included a resistive load bank with 15 settings (2.3 - 60Ω). During performance testing, a shore operator stepped through the load settings, maintaining each for a period of several minutes while recording current $I$ and voltage $V$ across the load bank at 1 Hz. Turbine angular velocity $\omega$ (rad/s) was calculated from voltage as $\omega=V/k$ where $k$ is a known generator-specific coefficient. All data sets were time stamped based on an internet synchronized time server.

The turbine hub height velocity profile, though spatially varied, is robust in time. In general, the reference velocity across the turbine rotor is a function of both space and time as

$$U_\infty = U_\infty(x, y, z, t). \tag{1}$$

For a fixed streamwise turbine location ($x$) and hub depth ($z$), given negligible vertical shear, this simplifies to a function of $y$ and time $t$. As the shear profile is relatively time-invariant over the testing period, a temporal average over a sufficient period approximates the lateral velocity profile as

$$\langle U_\infty \rangle = \langle U_\infty(y,t) \rangle \tag{2}$$

where the brackets denote a temporal average. To select a $\langle U_\infty \rangle$ representative of the flow across the entire turbine, a spatial average is calculated as

$$\overline{\langle U_\infty \rangle} = \overline{\langle U_\infty(y) \rangle} \tag{3}$$

where the over bar denotes a spatial average in lateral direction, excluding the region occupied by the generator and the drive shaft. From the time-averaged profile in Figure 2, the span of points from end-to-end of the rotor were linearly interpolated at 0.001 m resolution and then averaged to obtain a single, representative value.

From this temporally and spatially averaged free stream velocity, an effective tip speed ratio $\lambda$ and water-to-wire efficiency $\eta$ may be calculated as

$$\lambda = \frac{\omega R}{\overline{\langle U_\infty \rangle}} \text{ and} \tag{4}$$

$$\eta = \frac{\langle IV \rangle}{\frac{1}{2}\rho\alpha\overline{\langle U_\infty \rangle^3}A} \tag{5}$$

where $R$ is rotor radius (m), $\rho$ is water density (estimated 1000 kg/m$^3$), and $A$ is turbine rotor swept area (m$^2$). The cube of the temporal mean velocity has been corrected by $\alpha$=1.03 where

$$\alpha = \frac{\langle U_\infty{}^3 \rangle}{\langle U_\infty \rangle^3}. \tag{6}$$

to account for the difference between the mean of cubes (correct accounting) and cube of means (available information due to Doppler uncertainty). The correction factor ($\alpha$) was calculated empirically from a low-noise 16 Hz Doppler velocimeter.

### Results

Characteristic performance curves obtained from equations 4 and 5 during three sets of temporally discontinuous measurements are presented as Figure 4. There are small differences between curves indicating slight differences in mean stream velocity across the data collection period. The relative insignificance of these differences suggests that the time-invariant hypothesis is valid on times scales of days to weeks.

## IMPLICATIONS FOR TURBINE CONTROL

The characteristic performance curve in sheared flow presents obstacles for turbine control. Since the RivGen turbine has fixed-pitch blades, only generator torque can be used to regulate rotation rate. Below its rated power, the controller objective is to maximize the conversion of kinetic power to mechanical power ( “Region II” control [5]).

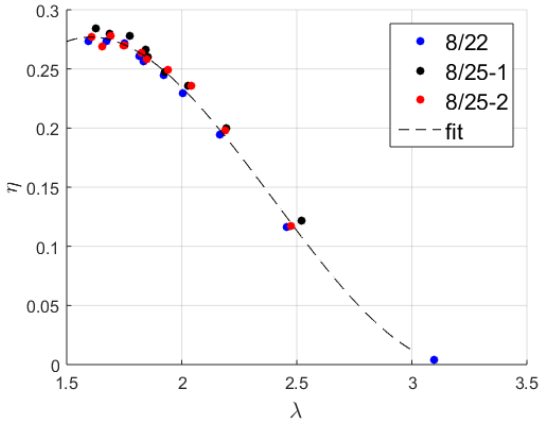


**FIGURE 4. PERFORMANCE CURVES AND THIRD ORDER POLYNOMIAL FIT**

**TABLE 1. TURBINE PARAMETERS FOR SIMULATION**

| Parameter | RivGen Turbine | TidGen Turbine |
|---|---|---|
| Rotor Swept Area ($m^2$) | 11.48 | 59.1 |
| Moment of Inertia ($kg*m^2$) | 277.5 | 2721.6 |
| Rotor Radius (m) | 0.7 | 1.4 |
| Damping coefficient estimate (N*m*s) | 0, 10, 20 | 50, 100, 150 |
| $K^*$ value | 140 | 5750 |

### Turbine Dynamics

The dynamics of a turbine can be described by

$$J\dot{\omega} = \tau_h - \tau_c - B\omega \qquad (7)$$

where $J$ is the turbine moment of inertia ($kg*m^2$), $\tau_c$ is control torque (N*m), $\tau_h$ is hydrodynamic torque (N*m), $B$ is damping coefficient (N*m*s), and $\omega$ is angular velocity (rad/s). The control torque is the free variable in the system. Hydrodynamic torque can be calculated as

$$\tau_h = \frac{1}{2}\rho A U_\infty^2 C_p / \lambda \ . \qquad (8)$$

If we assume the losses due to generator and drivetrain efficiency are constant over the range of operating angular velocities, $C_p$ can assumed to be approximated by $\eta$ because the shape of the curve, which dictates controller performance (Equation 11) will be unchanged. This allowed the third-order fit shown in Figure 4 to be used to determine $C_p$ as

$$C_p = 0.1363\lambda^3 - .9800\lambda^2 + 2.082\lambda - 1.096 \qquad (9)$$

for $1.5 < \lambda < 3.0$. At lower $\lambda$, the turbine was assumed to immediately stall. The instantaneous turbine shaft power $P_{rotor}$

$$P_{rotor} = \tau_c \omega \qquad (10)$$

is the power input (W) to the generator. Controller performance was simulated for the RivGen turbine, as well as the geometrically similar TidGen® turbine, which is designed for tidal environments. Turbine characteristics are presented in Table 1 and the characteristic performance of both turbines was assumed to be given by the polynomial fit.

### Simulation Architecture

A Matlab Simulink model was used to explore two different control architectures: linear proportional-integral tip speed ratio (PI-TSR) and non-linear maximum power point (MPP) control. The linear control is a feedback controller, while the non-linear controller is feedforward. Detailed discussion of these architectures is presented by Pao and Johnson [6] in the context of wind turbines. The PI-TSR controller attempts to maintain $\lambda=\lambda_s$, where $\lambda_s$ is the controller set point, by adjusting the control torque. The MPP controller adjusts the command torque as $K\omega^2$, where $K$ is a constant derived from the characteristic performance curve.

The metric used to compare control architectures and parameters is energy loss,

$$E_{loss} = 1 - \frac{\int P_{gen}(t)dt}{\int P_{\max}(t)dt} = 1 - \frac{\int \tau_c(t)\omega(t)dt}{\int \frac{1}{2}\rho A U_\infty^3(t) C_p^* dt} \qquad (11)$$

a ratio of actual controller performance to ideal controller performance. Low values of energy loss indicate a near-ideal controller, while high values indicate turbine stall.

The model numerically integrates the turbine hydrodynamic model described in the previous section for input flow velocity time series taken at two sites: the Kvichak River and Admiralty Inlet, WA. Because the turbine was found to be largely unresponsive to frequencies higher than 0.2 Hz, the input time series (16 Hz) were low-pass filtered. The simulation included user-defined noise for controller inputs. To simulate limitations on control actuation rate, command torque is updated at a user-specified rate.

### Results

The ideal $C_p^*$ occurs at $\lambda^* = 1.6$. This is close to the turbine stall condition. As a result, a turbine operating at the ideal point is vulnerable to stall if flow velocity decreases, particularly at slower control actuation rates. This trend is shown in Table 2, where stall prevention requires operating the turbine at non-ideal set-point ($\lambda_s$, $K_s$) for update

rates < 10 Hz. The range of values demonstrates the sensitivity of the controller to estimates for the damping coefficient. MPP control consistently outperforms PI-TSR control.

**TABLE 2. IMPACT OF TORQUE COMMAND UPDATE RATE FOR RIVGEN TURBINE IN KVICHAK RIVER**

| **Command Torque Update Rate** | **MPP (K*=140) Lowest Stable $E_{loss}$** | **PI-TSR (1.6=λ*) Lowest Stable $E_{loss}$** |
|---|---|---|
| 1/3 Hz | 28-31% ($K_s$=0.3 K*) | 64-90% ($\lambda_s$=1.5-1.6 λ*)(Stalls) |
| 1 Hz | 5-8% ($K_s$=0.6 K*) | 15-21% ($\lambda_s$=1.3 λ*) |
| 10 Hz | ~0-3% ($K_s$ ~ K*) | 0-3% ($\lambda_s$ ~ λ*) |

The TidGen turbine previously operated in Cobscook Bay with a MPP controller and command torque update rate of ~2000 Hz. Simulation results (not shown) suggest that this configuration should be stable with $E_{loss}$ ~ 0. However, in the field, stall occurred when K was more than 60% of optimal, resulting in $E_{loss}$ of ~20%. Given the rapid update rate, it is possible that the onboard measurement of ω contains noise. This was subsequently simulated to test this hypothesis. As shown in Table 3, noise level of 0.1 rad²/s² similar results to those observed in the field are obtained. Implementing a low-pass filter on this signal should improve controller performance. Because the turbine should have ~0 $E_{loss}$ with an update rate of 10 Hz, significant filtering should be possible.

**TABLE 3. IMPACT OF ANGULAR VELOCITY SIGNAL NOISE FOR TIDGEN TURBINE IN ADMIRALTY INLET FLOWS. 10 HZ UPDATE RATE**

| Rotation Rate Noise Variance (rad²/s²) | Non-linear Controller ($K^*$ ~ 5700) Lowest Stable $E_{loss}$ |
|---|---|
| 0 | ~0-1% ($K_s$~$K^*$) |
| 0.05 | 8-9% ($K_s$ = 0.6 $K^*$) |
| 0.1 | 13-16% ($K_s$ = 0.4 $K^*$) |
| 0.5 | 36-37% ($K_s$ = 0.2 $K^*$) |
| 1.0 | 42-43% ($K_s$ = 0.2 $K^*$) |
| 2.0 | 60-61% ($K_s$ = 0.1 $K^*$) |

### Control in Sheared Flow

PI-TSR control and other, more advanced control architectures, require information about inflow velocity [7], [8]. In sheared flow, this measurement will be spatially varying. A model of the RivGen turbine in the Kvichak shear flow (Figure 2) was constructed to consider the implications for point measurements.

### *Model Description*

For simulation, the turbine is subdivided into 0.001 m increments. The model assumes a span-wise constant ω with varying $U_\infty$, resulting in local variations in λ that translate to local variations in $C_P$. The performance curve given in Equation 9 is assumed to be valid for each rotor segment (i.e., no span-wise interaction between segments). Local values of λ < 1.5 are assumed to result in zero power production (i.e., this portion of the rotor span is assumed to be stalled). The model shows the aggregate power output from the turbine if performance is optimized at a specific span-wise location. The results are shown in Figure 5. The location along the rotor where λ should be set to maximize power generation is not simply the point of maximum velocity, but rather one that maintains local λ close to the global maxima for rotor sections in energetic flows. This is a function of shear profile, performance curve geometry, and turbine geometry (i.e., discontinuous rotor sections).

Non-ideal λ set points can produce the same maximum power output if they are defined at another location. This implies that a turbine can adjust to a changing shear profile by altering set point values, without spatially-resolved knowledge of the shear profile, by monitoring total power output for a given measured flow.

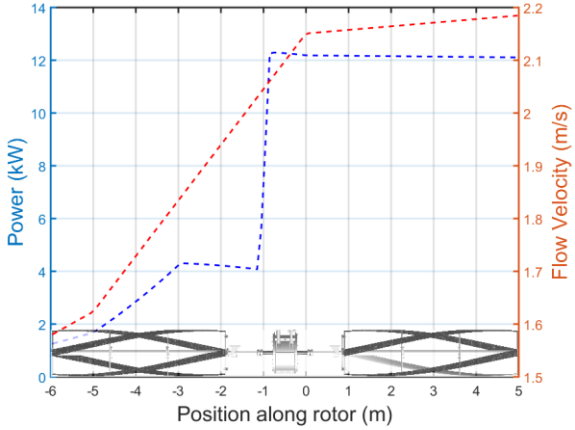


**FIGURE 5. AGGREGATE POWER OUTPUT FOR RIVGEN TURBINE IN SHEARED FLOW AS A FUNCTION OF THE POINT AT WHICH PERFORMANCE IS OPTIMIZED.**

## IMPLICATIONS FOR RESOURCE ASSESSMENT

Prior to deployment in Igiugig, AK, the RivGen turbine underwent tow trials that characterized the peak water-to-wire efficiency as ~20%. This is in-line with experimental performance of similar cross-flow turbines [9]. The maximum of the curve

in Figure 4 is 27%, a 35% increase in efficiency. If one were to assume a 20% maximum efficiency for the RivGen turbine, the observed power output would require an equivalent uniform inflow velocity of 2.3 m/s, which is higher than any velocity measured across the turbine. Blockage, calculated as

$$B = A/(A_r - A_s) \tag{12}$$

where $A_r$ is the cross-sectional area of the river in plane with the turbine axis and $A_s$ is the cross-sectional area of the turbine support structure, is an unlikely explanation for the improved performance as the turbine occupies only 3% of river cross-sectional area. However, vertical blockage of 20% may be significant. A visible free-surface deformation occurs during operation just downstream of the turbine. This suggests that the vertical blockage or surface proximity may allow the turbine to harness momentum from adjacent faster-flowing areas. To quantify this, it is recommended that resource assessment activities include flow measurements taken both pre- and post- installation.

## CONCLUSION

Point measurements of inflow velocity cannot provide conclusive turbine power-performance curves in sheared flow. Rather, an array of point measurements are needed to spatially resolve the shear flow profile. If the profile is shown to be synoptic over the time-scales of the power output characterization, temporally and spatially averaged inflow velocities used to calculate averaged forms of the non-dimensional performance coefficients ($\lambda$ and $\eta$) produce consistent performance curves.

Generally, the closeness of $\lambda^*$ to the stall regime of the turbine increases controller vulnerability to turbulence, signal noise, and slow torque update rates, necessitating more conservative set points for stable operation. Velocity shear has implications for turbine control schemes. Defining a representative reference velocity will be a challenge for any control strategy that depends on knowledge of free-stream velocity.

## ACKNOWLEDGEMENTS

Support from the Alaskan field crew (Joe Talbert, Alex deKlerk, Curtis Rusch, Ryan Tyler, and Monty Worthington), ILC camp, D'nina Air Taxi, and the village of Igiugig is gratefully acknowledged.

## REFERENCES

[1] Kilcher L. F., and Thomson J., 2014, "Determining the Spatial Coherence of Turbulence at MHK Sites," *Proceedings of the 2nd Marine Energy Technology Symposium,* Washington, DC. pp. 1–7.

[2] Thomson J., Polagye B., Durgesh V., and Richmond M. C., 2012, "Measurements of Turbulence at Two Tidal Energy Sites in Puget Sound, WA," *IEEE J. Ocean. Eng.*, **37**(3), pp. 363–374.

[3] Neary V. S., Gunawan B., and Sale D.C., 2013 "Turbulent inflow characteristics for hydrokinetic energy conversion in rivers," *Renew. Sustain. Energy Rev.*, **26**, pp. 437–445.

[4] Thomson J., Kilcher L., Richmond M., Talbert J., DeKlerk A., Polagye B., Guerra M., and Cienfuegos, R., 2013, "Tidal Turbulence Spectra From a Compliant Mooring," *Proceedings of the 1st Marine Energy Technology Symposium*,. Washington, DC.

[5] Laks J. H., Pao L. Y., and Wright, A. D., 2009, "Control of Wind Turbines : Past , Present , and Future," in *American Control Conference*, St. Louis, MO, pp. 2096–2103..

[6] Pao L. Y. , and Johnson K. E., 2009, "A Tutorial on the Dynamics and Control of Wind Turbines and Wind Farms," in *American Control Conference*, St. Louis, MO.

[7] Harris M., Hand M., and Wright A., "Lidar for Turbine Control, 2005," *NREL Tech. Rep.*, NREL/TP-50. NREL, Golden, CO.

[8] Boukhezzar B., Siguerdidjane H., and Hand, M. M., 2006,"Nonlinear Control of Variable-Speed Wind Turbines for Generator Torque Limiting and Power Optimization," *J. Sol. Energy Eng.*, **128**(4), pp. 516-530.

[9] Bachant, P. and Wosnik, M., 2015, "Performance Measurements of Cylindrical- and Spherical-Helical Cross-Flow Marine Hydrokinetic Turbines , With Estimates of Exergy Efficiency," *Renew. Energy*, **74**, pp. 318–325.